12-1-2011

A computational study of electronic structures of graphene allotropes with electrical bias

James Edward Nathaniel II
Clark Atlanta University

ABSTRACT

DEPARTMENT OF PHYSICS

NATHANIEL II, JAMES E. B.S. MOREHOUSE COLLEGE, 2008

A COMPUTATIONAL STUDY OF ELECTRONIC STRUCTURES OF GRAPHENE ALLOTROPES WITH ELECTRICAL BIAS

Committee Chair: Xiao-Qian Wang, Ph.D.

Thesis dated December 2011

Graphene is a two-dimensional system consisting of a single planar layer of carbon atoms with hexagonal arrangement. Various approaches have been proposed to control its physical and electronic properties. When appropriately cut, rolled, and bonded, graphene generates single-walled carbon nanotubes of varying diameters. Graphite intercalation compounds are materials formed by inserting molecular layers of compounds between stacked sheets of graphene. We have studied the physical and electronic responses of two graphene layers intercalated with $FeCl_3$ and of metallic, semi-metallic and semiconducting nanotubes when normally biased using electric fields of various magnitudes. By means of first-principles density functional calculations, our results indicate that the band structures of the aforementioned graphene structures are modified upon application of a bias voltage. In the case of nanotubes, electric biasing allows tuning of the band gap leading to a transition from semiconducting to metallic state, or vice versa. In the case of the $FeCl_3$ intercalant compounds, electric biasing results in shifting of the Dirac point.

A COMPUTATIONAL STUDY OF ELECTRONIC STRUCTURES OF GRAPHENE ALLOTROPES WITH ELECTRICAL BIAS

A THESIS

SUBMITTED TO THE FACULTY OF CLARK ATLANTA UNIVERSITY

IN PARTIAL FULFILLMENT OF THE REQUIREMENTS FOR

THE DEGREE MASTER OF SCIENCE

BY

JAMES E. NATHANIEL II

DEPARTMENT OF PHYSICS

ATLANTA, GEORGIA

DECEMBER 2011

ACKNOWLEDGMENTS

The work presented here would not have been possible without the support and guidance of several people, but all honor must be given to the Lord, my shepherd. A sincere thank you goes to my parents, my soul mate and my family for their tireless belief in me. I would like to express my appreciation to my advisor Dr. Xiao-Qian Wang, for his invaluable guidance, direction and supervision throughout the tenure of my study. I also acknowledge the support given by the academic staff of the Clark Atlanta University Department of Physics, and Dr. Alexis Nduwimana who helped me throughtout various projects. A sincere thanks goes to Dr. Alfred Msezane for being a committee member. I wish to thank my colleagues Dr. Olayinka Ogunro, Kelvin L. Suggs, Duminda K. Samarakoon, Cherno B. Kah, Vernecia N. Person, Chantel I. Nicolas, Rosi N. Gunasinghe, Kregg D. Quarles and all the members of the research group whose assistance, perception and advice influenced production and made the office an enjoyable place to work. I am grateful for the finacial support from the National Science Foundation (Grant No. DMR-0934142).

TABLE OF CONTENTS

PAGE

LIST OF FIGURES

LIST OF TABLES

LIST OF ABBREVIATIONS

BLYP	Becke-Lee-Yang-Parr
CBM	Conduction Band Minimum
CBM-1	Conduction Band Minimum -1
CNT	Carbon Nanotube
DFT	Density Functional Theory
DN	Double Numerical
DND	Double numerical with *d* polarization
$FeCl_3$	Ferric Chloride
FLG	Few Layer Graphene
FLGIC	Few Layer Graphene Intercalation Compound
GGA	Generalized Gradient Approximation
GIC	Graphene Intercalation Compound
PBE	Perdew, Burke, and Ernzerhof
SLG	Single Layer Graphene
SWNTs	Single-Walled Carbon Nanotubes
TS	Tkatchenko-Scheffler
VBM	Valence Band Maximum
VBM+1	Valence Band Maximum +1

CHAPTER 1

1. INTRODUCTION

Graphene is a two-dimensional system consisting of a single planar layer of carbon atoms with hexagonal arrangement. Graphene is an emerging material for applications in technology. The next wave of electronics could benefit from graphene's excellent electric field effect on transport properties and massless Dirac fermion like charge carriers (*1-3*). As a zero-gap semiconductor, graphene possesses a number of outstanding electronic properties such as tunable carrier-type and density, exceptionally high carrier mobility, quantization of the conductivity, and fractional quantum Hall effect even at room temperature (*2-7*). These intrinsic qualities are reasons for intensive experimental and theoretical investigations.

Much progress has been made in recent years pertaining to the discovery of graphene's unique structural and electronic qualities, the methods of fabricating graphene in various forms (such as nanoribbons, carbon nanotubes, sheets, etc.), and in controlling its properties. High carrier mobility makes graphene an ideal material for nanoelectronic applications, but mass-controlled production of graphene and graphene-based structures has fallen short of precision (*2, 6, 7*). Expertise in fabrication is a necessity, and the ability to manipulate and control the properties of existing structures is also essential. In

developing semiconductors it is desirable to have an energy gap; being able to create a gap and fine-tuning the gap size is even more advantageous. Many of the unique properties of graphene are attributed to a single layer of graphene. This notwithstanding, it is advantageous to modify graphite or few layers of stacked graphene such that they behave as a single layer (*8*).

Various methods and combinations of methods are used to functionalize graphene and its allotropes, such as affixing polymer chains or hydrogen atoms to the structure. In this study we used electrical bias as a means to dope structures. The goal of this work is not only to understand electrical bias and the mechanism driving the process, but also to study the effects of electrical biasing on different compounds. Chapter 1 of this thesis introduces the topic and states the purpose of the endeavor. Chapters 2 and 3 provide the background on the structures studied, the methodology and discussion of results related to the structural and electronic properties of the biased nanotubes and intercalated graphene, respectively. In Chapter 2, metallic, semi-metallic and semiconducting single-walled carbon nanotubes were studied with electrical bias. In Chapter 3, a unique structure composed of two layers of graphene intercalated with ferric chloride ($FeCl_3$) was investigated with the application of an electrical bias. Chapter 4 merely wraps up our findings and confers about future work.

CHAPTER 2

2. ELECTRONIC MODIFICATIONS OF SINGLE-WALLED CARBON NANOTUBES VIA ELECTRIC BIAS

2.1 Introduction

Single-walled carbon nanotubes (SWNTs or SWCNTs) are a carbon allotrope of one dimension that exhibits special electronic properties (*9*). Electrons are confined to travel in a single direction (paraxial to the tube); hence referred to as one-dimensional semiconducting and conducting nanowires. A single-walled carbon nanotube can be described as a graphene sheet rolled into a cylindrical shape. The structure is one-dimensional with axial symmetry, and in general exhibits a spiral conformation (*10*). SWNTs are labeled in terms of graphene lattice vectors.

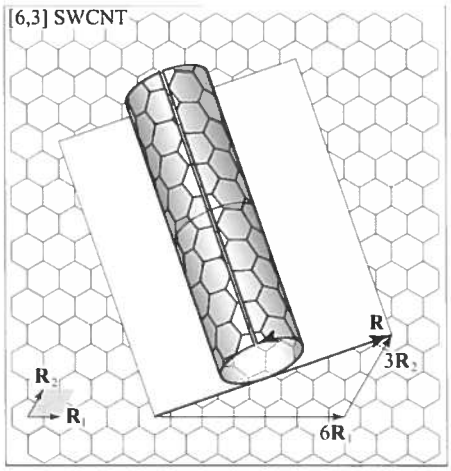

Figure 2.1 Mapping of a graphene sheet to create (6,3) SWNT. The unit cell of the graphite lattice is the gray rhomboid in the lower left corner and defined by the primitive lattice vectors $\mathbf{R}_1$ and $\mathbf{R}_2$ [9].

As seen in Figure 2.1, the Bravis lattice vector **R**, is defined in terms of two primitive lattice vectors $\mathbf{R}_1$, $\mathbf{R}_2$ and a pair of indices, (n_1,n_2), where the established relationship is as follows (*10*):

$$\mathbf{R} = n_1\mathbf{R}_1 + n_2\mathbf{R}_2 \equiv (n_1,n_2) \qquad (2.1)$$

The (n_1,n_2) notation is commonly known as the chiral index; n_1 and n_2 must be integers. The chiral index may be used to uniquely identify SWNTs (*10*).

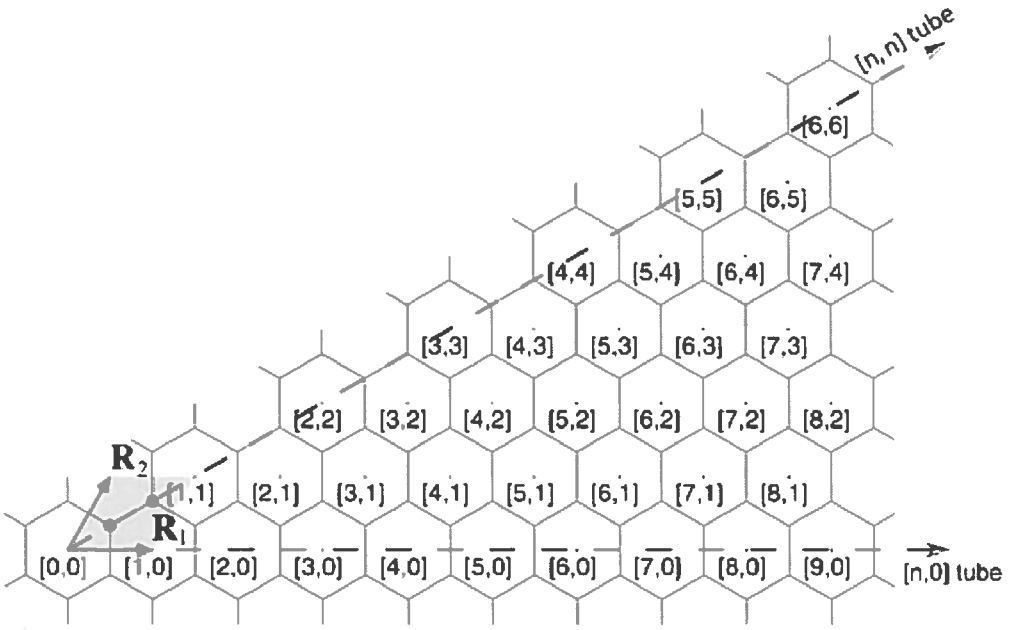

Figure 2.2 Primitive lattice vectors are shown on the left near the origin (0,0). Chiral indices are enclosed in brackets.

There are three types of SWNTs: armchair (n, n), zigzag $(n,0)$ and chiral nanotubes $(n_1, n_2 \neq n_1 \neq 0)$ (*11*). The resultant type of nanotube depends on how the

graphene sheet is rolled. The nomenclature is a consequence of the shape of the carbon bonds on the outer edges of the nanotube. Zigzag and armchair tubes are achiral. Armchair tubes have C-C bonds normal to the tube axis. Conversely, zigzag tubes have C-C bonds parallel to the tube.

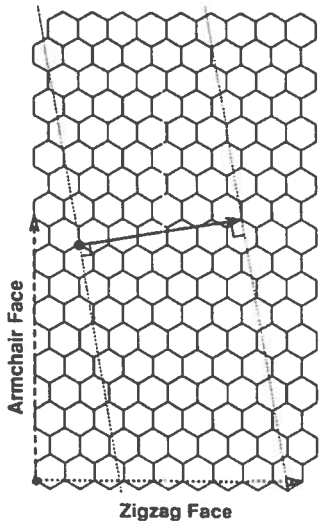

Figure 2.3 Model of armchair and zigzag nanotubes from a graphene sheet, armchair versus zigzag edges illustrated (*12*).

The electrical properties of a nanotube depend on its structure. This is due to the symmetry and unique electronic structure of graphene. For SWNTs with chiral indices (n,m), where $n = m$ the nanotube is metallic; if $n - m$ is divisible by 3 the nanotube is semimetallic, meaning that it has a very small band gap (greater than 0 eV but significantly less than 1 eV); otherwise nanotubes are semiconducting. For example all armchair nanotubes, such as (6,6) are metallic, (15,0) and (9,3) are semimetallic and SWNTs (6,4) and (13,0) are semiconducting (*13*).

2.2 Method

The structural and electronic properties of all conformations in this study were investigated using first-principles, density functional theory (DFT) calculations. In physics, using quantum mechanics is typical to examine a system of molecular size. This approach requires one to solve the Schrödinger equation by applying the Hamiltonian to wave functions central the structure. This technique is fine for dealing with a particle in a box, but when observing many-body compounds that construct solids, this method tends to be tedious, laborious, complex and time-consuming.

The structure and properties of matter are governed by electron-electron interactions. Compared to using the complicated wave function, the total electron density $\rho(\mathbf{r})$ of a structure, which only depends on three position variables, x, y, and z, is more appropriate to handle when running molecular calculations (*13, 14*). The foundation of DFT is that there exists a relationship between the total energy of a system and the electron density. The Hamiltonian depends on the positions of the nuclei, their atomic numbers and the total number of electrons. DFT uses the fact that the electron density establishes many properties of a system, such as the ground-state energy; meaning the total energy E is a functional, a function of a function, of the electron density (*15*). DFT is based on the electron distribution as a basic variable rather than tackling the multifaceted wave function consisting of many individual terms (*16*). The DMol^3 code includes static potentials from an externally applied electric field used for electric bias. The Hamiltonian is composed of the potential arising from the external electric field ($E_{ext.}$), kinetic energy operator T, and Hatree (V_H) and exchange-correlation (V_{xc})

potentials. DMol^3 is widely used in molecular systems to study the effects of electric field on reactivity, hyperpolarizability, work function, and field-emission (*17-20*). Furthermore, the Hamiltonian can be extended to a periodic system for studying the effects of a uniform constant external electric field on conductance, geometry, energy barrier, electron-trapping, and energy band gap (*21-27*).

Our calculations are based on DFT with generalized gradient approximation (GGA) for exchange and gradient-corrected Becke-Lee-Yang-Parr (BLYP) parametrization used in DMol^3 package (*28-31*). Double numerical with *d* polarization (DND) basis sets were implemented (*22*). The optimization of atomic positions proceeded until the forces were less than 0.01 eV/Å and the change in energy was less than 5×10^{-4} eV. A kinetic energy cutoff of 280 eV in the plane-wave basis and integrations over reciprocal space are based on Monkhorst-Pack scheme with *k*-points ($1\times 1 \times 8$ for nanotubes) sampling 0.05 Å^{-1} separation in the Brillouin zone. These parameters were selected such that sufficient convergence of the charge density to the grid is achieved (*32, 33*). All our calculations have been carried out using periodic boundary conditions to simulate an infinite nanotube. The vacuum space varied from 15-20 Å as necessary to accommodate the cylindrical circumferences of nanotubes of ranging sizes. Vacuum space is necessary to avoid interactions between mirror images of the structure. The orbital cutoff was set to be global and with a value of 3.4 Å. The atoms were fitted to the highest reasonable degree of symmetry.

The (12,0), (13,0), (14,0), (6,6), and (6,4) nanotubes were studied by applying a static electric field parallel to the axel of the tubes. For each nanotube, the magnitudes of the electric field were varied in observing band gap tunablity.

2.3 Results and Discussion

Electric bias of nanotubes presents an approach for altering some of the properties associated with nanotubes, such as charge distribution. Controlling electric characteristics of nanotubes can create unique properties in nanotubes not typical with a particular variety. Methods such as electric bias may be used to optimize functionality of SWNT by altering the mechanical, chemical, and electrical properties. Electric bias occurs via non-covalent electrostatic interactions accomplished by applying an electric field to the system. Electric fields were applied parallel to tube axis, in the *z*-direction.

Figure 2.4 illustrates the nanotubes used in the study: the (6,4), (6,6), (12,0), (13,0), and (14,0). These structures are not modified from their usual configuration. A geometry optimization using force field-based molecular dynamics was performed first, followed by optimization using first-principles density functional calculations on each biased confirmation to reach the most stable state (*22*). First-principles calculations are independent to the assignment of bonds, whereas the energy of classical force field-based calculations depends on the type of inter-atomic bonds.

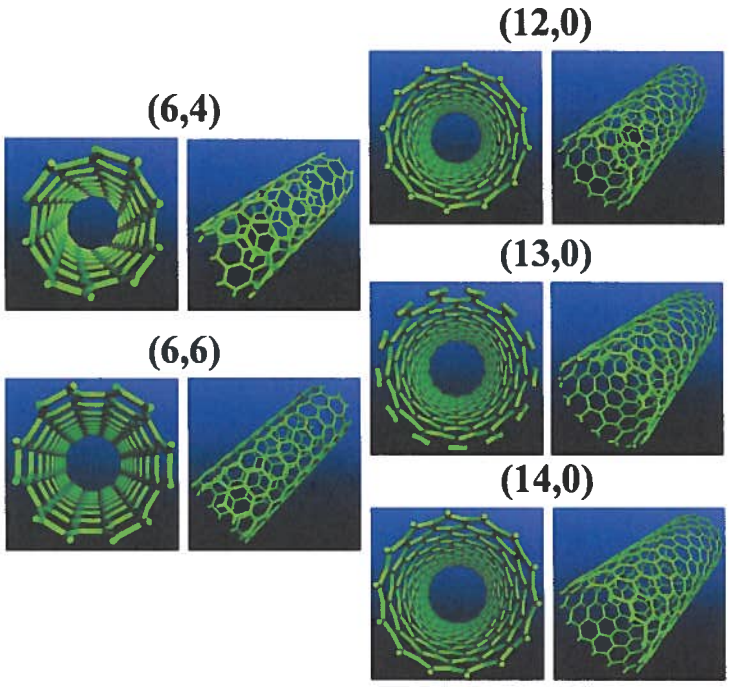

Figure 2.4 Stick rendering of (6,4), (6,6), (12,0), (13,0), and (14,0) nanotubes (left: top view; right: perspective view).

As seen in Figure 2.4, the confirmations are similar but differ in radial width and bond locations. The energies of all the structures were calculated along with the energy gap between the conduction band minimum (CBM) and the valence band maximum (VBM). Summarized in Table 2.1 are the calculated total energies, band gaps, and electric field magnitudes for each structure.

Table 2.1 Calculated total and binding energies, and band gaps for nanotubes with electric bias.

	electric field magnitude (V/Å)	*total energy (eV)*	*binding energy (eV)*	*band gap (eV)*
(6,4)	0	-157509.7132	-1083.01294	1.1152
	0.51421	-157557.1843	-1130.484055	0.8432
	1.54263	-158359.2943	-1932.593951	0.0272
(6,6)	0	-24871.33742	-172.3847328	0.0816
	2.57105	-24877.24128	-178.2886288	0.2992
	10.2842	-24967.68254	-268.7298474	0.544
(12,0)	0	-49744.04549	-346.140128	0.1632
	1.54263	-49756.51283	-358.6074765	0.2992
	2.57105	-49778.30335	-380.3979949	0.6528
(13,0)	0	-53870.21788	-355.820404	0.6528
	1.02842	-53939.47588	-425.078404	0.3536
	1.54263	-54299.73637	-785.3389061	0
(14,0)	0	-58036.38481	-405.495239	0.7888
	2.57105	-58076.03145	-445.1418774	0.3264
	4.11368	-58137.15643	-506.2668571	0.0272

Table 2.1 indicates the conversion of metallic and semi-metallic nanotubes into semiconducting nanotubes, and vice versa. This is evident by comparing the band gaps of the pristine structures to the band gaps of the acutely biased structures. The effect of the electric field can be studied by adding a potential via the nuclear charges. Our calculations show that the (6,4) tube closes to a gap of ~ 0.027 eV to by an electric bias of ~1.54 V/Å, while the (6,6) tube opens to a gap of ~0.54 eV by an electric bias of ~10.28 V/Å. The (12,0) tube opens a gap of ~0.65 eV by an electric bias of ~2.57 V/Å, while the (13,0) tube closes a gap to ~ 0.0 eV by an electric bias of ~1.54 V/Å. Finally, the (14,0) tube closes to a gap of ~ 0.027 eV by an electric bias of ~4.11 V/Å. When the electric bias is further increased, the resultant gaps tend to return back to their original

state, and the system turns back to either metallic/semi-metallic or semiconducting, respectively. We show in Figure 2.6 the calculated band structures for the nanotubes studied. For example, Figure 2.6 depicts the band gap of (6,4) decreasing monotonically from about 1.13 eV to 0.03 eV with increase of electric bias. The critical bias for converting (6,4) from semiconducting to semi-metallic is estimated to be about 1.54 V/Å.

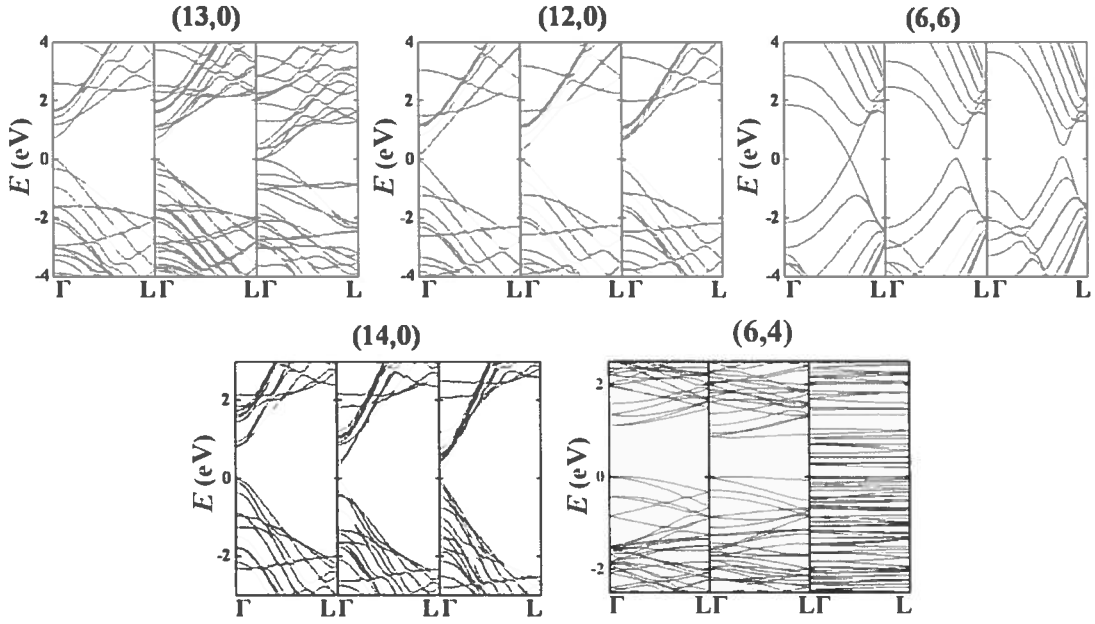

Figure 2.5 Calculated band structures of single-walled carbon nanotubes: electric bias increases from left to right, starting with no electric bias. The Fermi level is set to 0 eV.

Shown in Figure 2.6 are the charge densities corresponding to the pristine and the biased nanotubes. The charge densities shown are representative of the valence band maximum (VBM) and the conduction band minimum (CBM). In the absence of bias, the charge density distributions are symmetrical both in conduction and valence bands. With the application of an electric bias, charges transferred into the conduction and valence

bands act in a concerted fashion, resulting in charge accumulation and depletion in the conduction and valence bands, respectively.

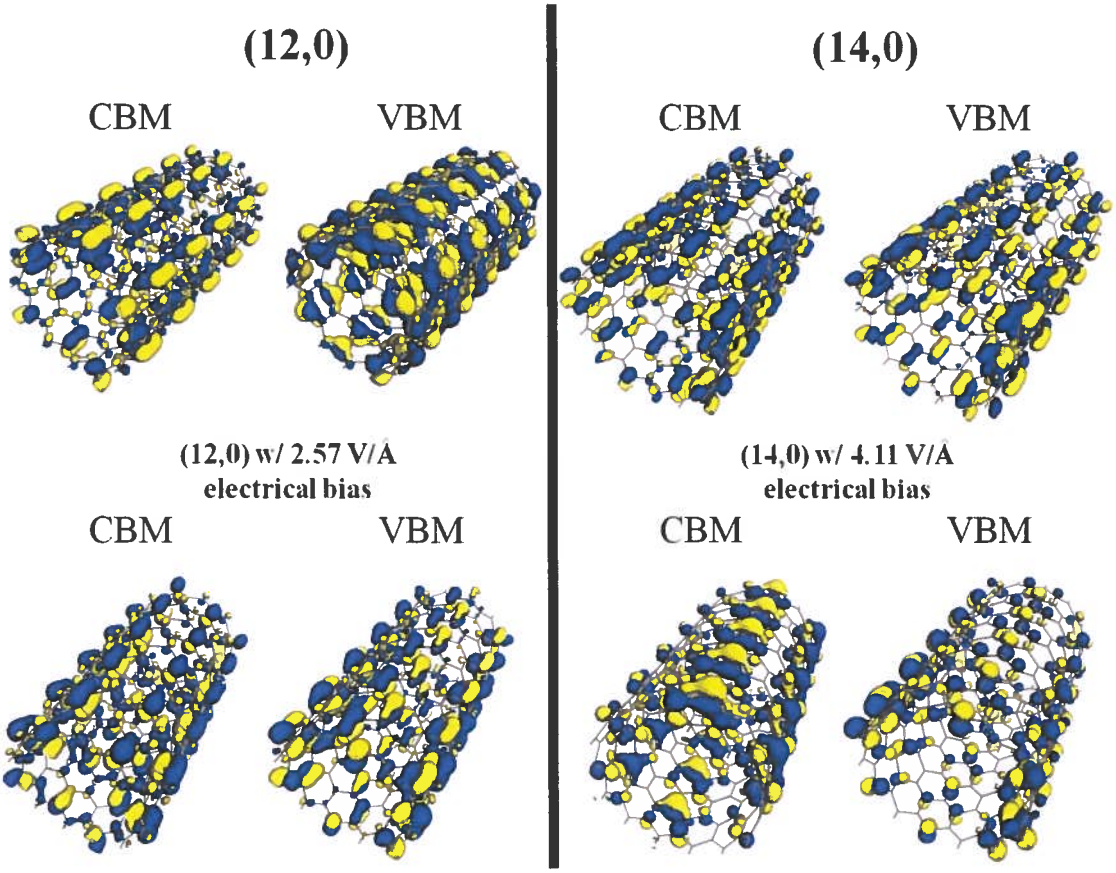

Figure 2.6 Calculated charge density distributions for (12,0) and (14,0) SWNTs at the band center of the corresponding conduction and valence band states with no bias and critical electric bias, respectively.

2.4 Conclusion

In summary, we have studied the electronic characteristics of biased metallic, semi-metallic, and semiconducting SWNTs. The resultant structures are modified and the electric bias method can be employed to fine-tune structural electronic properties. Our findings demonstrate the ability to continuously tune carbon nanotube band gaps by

gauging an electric field. Electronic properties generally determine transport and optical properties. Being able to tune the band gaps of nanotubes enables flexibility and optimization of graphene-based structures to be used in nanodevices.

CHAPTER 3

3. ELECTRONIC MODIFICATIONS OF ELECTRICALLY BIASED $FeCl_3$ BASED INTERCALATED TWO LAYER GRAPHENE

3.1 Introduction

Graphene has had the world of semiconductors stirring about the promising possibilities. Graphene, a single layer of carbon atoms with hexagonal arrangement, has attracted enormous interest due to its excellent field-effect transport properties and massless Dirac fermion like charge carriers (*1-3*). However, many of the unique properties of graphene are exclusive to single layer graphene (SLG). Given the complexity in the mass production of SLG, it would be very desirable to modify few layer graphene (FLG) samples so that they have properties similar to those of SLG.

In efforts to make graphene useful, various approaches have been proposed to tailor its physical and electronic properties. Graphene intercalation compounds (GICs) are complex materials that form by insertion of molecular layers of different chemical species between graphite layers (*34*). The interlayer distance of graphite is dramatically increased due to the presence of intercalants. The additional distance strongly affects the electronic coupling between graphene layers, thereby changing its properties. Different electrical, thermal, and magnetic properties can be achieved for GIC by simply choosing

from various intercalants (*34-36*). As such, intercalation of graphene-based compounds is an efficient method to modify the properties of FLG.

We report in this chapter that in graphene-based intercalation compounds, applying electrical bias allows for further control of the electronic characteristics. $FeCl_3$ (ferric chloride) intercalated FLG has been successfully prepared by two-zone vapor transport method (*8*). We have calculated the band structure and investigated the associated charge densities for electrically biased two-layer graphene intercalated with $FeCl_3$.

Few layer graphene intercalated compounds (FLGICs) band structure is similar to that of single layer graphene but with strong doping effect due to the charge transfer from graphene to $FeCl_3$ (*37*). The flat bands of the GIC originate from the *d* orbital of iron. The band structure of GIC and single layer graphene are very similar except for those bands. The Dirac point of SLG is located exactly at the Fermi surface while that of the GIC is located at ~1 eV, suggesting that GIC is strongly hole doped. $FeCl_3$ is considered as an acceptor in the charge transfer induced doping effect in the $FeCl_3$-FLGIC (*38*). Fully intercalated $FeCl_3$-FLGIC can be interpreted as quasi-individual graphene layers superimposed one on the other with very weak coupling effect through the intercalant layers. The electronic properties of FLGIC behave like those of SLG with linear dispersion near the Dirac point (*39*). Interaction between $FeCl_3$ and graphene is minimal; each layer proceeds as a decoupled doped monolayer (*39*). The main effect of $FeCl_3$ intercalation is the introduction of strong charge transfer doping and an increase of the distance between layers of stacked graphene. The combination of these effects results in

the electronic structure of $FeCl_3$-based FLGIC closely resembling that of SLG. The effects of intercalating FLG using different intercalants suggest a promising method to achieve desirable properties for FLG in future applications.

3.2 Method

The structural and electronic properties of all conformations in this thesis were investigated using first-principles DFT calculations. A description of DFT can be found in Chapter 2, Section 2.2. The GIC structure consists of two graphene sheets sandwiching ferric chloride, as shown in Figure 3.1. A supercell with lattice constants $a = b = 12.12$ Å and $c = 9.370$ Å was constructed, with 2×2 periods of FeCl3 and 5×5 unit cells of graphene as suggested by previous works (*8*). $FeCl_3$ was constructed as delineated by Dresselhaus and coworkers (*34*). The DFT calculations were based on semiempirical dispersion corrected generalized gradient approximation (GGA), exchange-correlation functional Perdew, Burke, and Ernzerhof (PBE), and rectified by dispersion-correction scheme of Tkatchenko-Scheffler (TS) (*22, 40*). Currently, the correct long-range interaction terms are not present in the majority of most popular DFT functionals. Non-covalent forces, such as van der Waals interactions and hydrogen bonding, are essential for the formation and function of molecules and materials. The TS scheme employs semiempirically determined homonuclear parameters. The missing dispersion contribution to the interatomic interaction is approximated by a simple isotropic potential. TS correction exploits the relationship between polarizability and volume, which accounts for the relative variation in dispersion of differently bonded atoms. The

dispersion correction is achieved by weighting values taken from the first-principles database with atomic volumes derived from Hirshfeld partitioning of the electronic density (*22*).

A conjugate gradient algorithm with a force convergence criterion of 0.001 eV/Å optimized the structure, and *k*-points (1× 1 × 2) sampling with 0.05 $Å^{-1}$ separation in the Brillouin zone are used. Double numerical (DN) basis sets were implemented (*22*) and the optimization of atomic positions proceeded until the forces were less than 0.001 eV/Å and the change in energy was less than 5×10^{-4} eV (*33, 34*). Calculations were carried out using periodic boundary conditions. The vacuum space of 9.416 Å separating periodic graphene sheets was necessary to avoid interactions between replicas. The orbital cutoff was set to be global and with a value of 3.4 Å. The structure has P-31M (D3D) symmetry.

A static electric field was applied perpendicular to the graphene layer plane. Electric field magnitudes were changed from 0 to 2.06 V/Å.

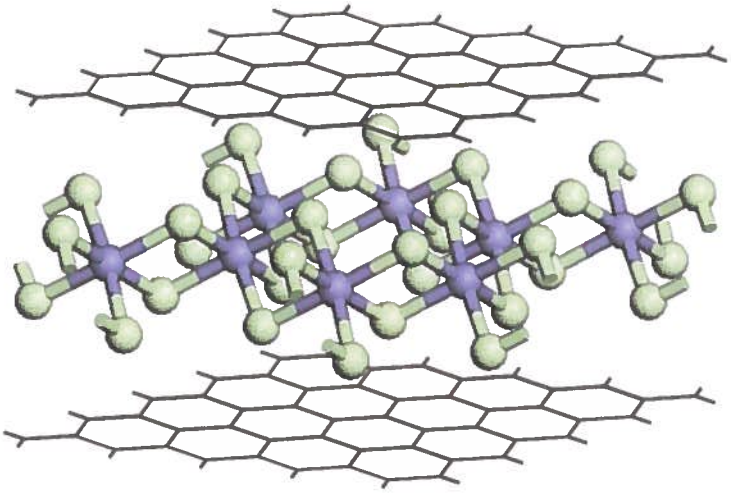

Figure 3.1 Crystal structure of two layers of graphene intercalated with $FeCl_3$. The graphene layers, denoted by gray, sandwich $FeCl_3$; Cl atoms and Fe atoms are denoted as green and blue, respectively.

3.3 Results and Discussion

Applying electric bias on graphite intercalated compounds presents an approach for modifying few-layer graphite flakes to behave more similarly to single-layer graphene, and possibly to achieve distinct structural and electric properties. Functionalization of GICs can create unique properties in compounds and may be used to optimize the physics and chemistry by altering the mechanical, chemical and electrical properties. Electric bias functionalization occurs via non-covalent electrostatic interactions brought about by applying an electric field to the system. The electric fields were applied normal to the graphene plane, in the *z*-direction.

The energies of the pristine and doped structure have been calculated along with the band structures. Figure 3.2 depicts the calculated band structures of $FeCl_3$-FLGIC

demonstrating the modification achieved by applying an electric bias. The magnitude of the electric field increases from left to right, with the pristine structure on the far left.

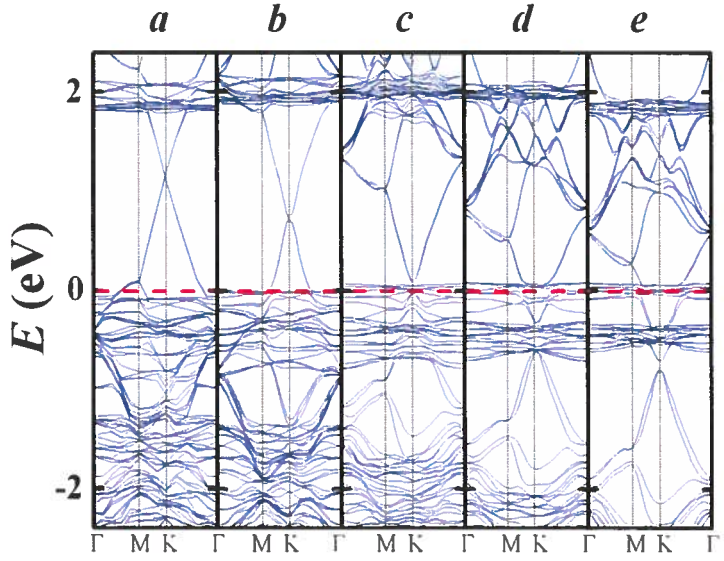

Figure 3.2 Calculated band structures of two layers of graphene intercalated with $FeCl_3$. (a) no electric bias, (b) 0.51 V/Å electric bias, (c) 1.03 V/Å electric bias, (d) 1.54 V/Å electric bias, and (e) 2.06 V/Å electric bias.

Figure 3.2 clearly indicates that the Dirac point, represented by the crossings, is shifting downwards as the electric field magnitude increases. It is of interest to observe the two sets of flat bands in the pristine graphene labeled ***a***: around 2 eV and from ~0 to -0.8 eV. Comparing band structures ***a*** through ***e***, it is clearly noticeable that the flat bands originating from the $FeCl_3$ are shifting upwards and contracting as the electric bias increases in magnitude. The effect of the electric field can be studied by adding a potential via the nuclear charges. Our calculations show that the Dirac point for the pristine GIC is at ~1 eV, in accord with the results in previous calculations (*8*). The electric bias of 0.51 V/Å shifts the Dirac point to about ~0.8 eV; the electric field of 1.03

V/Å in magnitude shifts the Dirac point almost to the Fermi level at 0 eV. Increasing the electric field to 1.54 V/Å in magnitude shifts the Dirac point to ~ -1 eV; and the electric field at 2.06 V/Å in magnitude, the Dirac point shifts to ~ - 2 eV. However, when the electric bias is further increased, the Dirac point shifts back towards the original state.

The downshift of the Dirac point and upshift of the flat bands is a result of charge transfer. The unbiased $FeCl_3$-graphene compound is hole-doped, establishing the Dirac point about ~1 eV above the Fermi level. The introduction of electrical bias to the system excites electrons from the graphene layers' conduction band to the ferric chloride's valence band; as two electrons leave a graphene band they join a $FeCl_3$ band. This occurrence is continuous as electric bias increases, pushing the ferric chloride flat bands higher as the graphene's Dirac point decreases. This method can be used to control the hole doping of the $FeCl_3$ intercalation, resulting in a *n*-type doping affect.

The flat bands in the band structure are near gap states. The corresponding charge densities for a few near gap states of the pristine structure, the valence band maximum (VBM), one band below the valence band maximum (VBM-1), conduction band minimum (CBM) and one band above the conduction band (CBM+1), are depicted in Figure 3.3. The charges for the flat bands are primarily confined to the $FeCl_3$ layer. This is in conformity with the band structure in Figure 3.2. It is worth noting that the Dirac linear dispersion from the graphene remains intact, as does the flat bands from the $FeCl_3$. The effect of the electric bias on the band structure is solely manifested in a systematic shift in the Dirac point and flat bands.

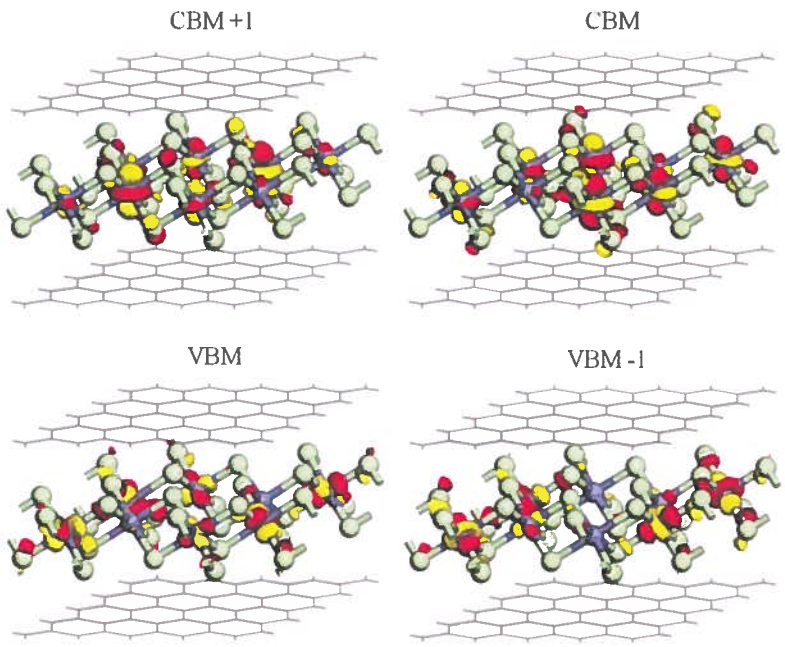

Figure 3.3 Extracted charge density distribution at the band center of the corresponding conduction and valence states in the pristine structure.

Table 3.1 Calculated total energies, binding energies, and Dirac point associated with the electric bias magnitude applied to $FeCl_3$-FLGIC.

Electric Bias Magnitude (V/Å)	*Dirac Point (eV)*	*Total Energy (eV)*	*Binding Energy (eV)*
0	~1.0	-678866.247	-886.206
0.514	~0.8	-678889.923	-909.882
1.028	~0.0	-678992.87	-1012.829
1.543	~ -1.3	-679190.907	-1210.866
2.057	~ -1.9	-679545.057	-1565.017

Table 3.1 presents the total and binding energies of the structures, as well as where the Dirac point is associated with the electric bias magnitudes. Table 3.2 presents

the distances between layers per electric bias magnitude. It is worth mentioning that the structure expanded continuously as the electric bias increased. The $FeCl_3$ stretched getting closer to the graphene layers flanking it on both sides, while the graphene sheets actually repelled from each other.

Table 3.2 Distances between graphene and $FeCl_3$ layers with electric bias magnitude

Electric Bias Magnitude (V/Å)	Distance Between Graphene and FeCl3 (Å)	Distance Between Graphene Sheets (Å)
0	4.689	9.405
0.514	4.688	9.409
1.028	4.683	9.416
1.543	4.682	9.423
2.057	4.677	9.426

3.4 Conclusion

In conclusion, our results show that while introducing $FeCl_3$ as an intercalant between graphene sheets produces strong charge transfer and chemical doping, further electrical tuning can be achieved by application of electric bias. We are the first to document this phenomenon discovered using first principle calculations. Few-layer graphite intercalate compounds are quite promising materials not only because of the modification of the graphene electronic structure, but also the possible modification of electrical, thermal, and magnetic properties with choice of different intercalants. The ability to control doping levels is much sought after for semiconductors. One of the many potential applications of this method is in the fabrication of transistors; *p-n* junctions could be created with simple applications of electric fields. The transistor is often

regarded as one of the most influential inventions of the last century. The implementation of graphene and graphene modification techniques can open up new worlds of possibilities in transistors and semiconductors in general.

CHAPTER 4

4. CONCLUSIONS AND FUTURE WORKS

In the last two chapters, we have presented calculations and results of allotropes of carbon both in pristine condition and having been subjected to electric bias. Specifically, in Chapter 2 we focused on various metallic, semimetallic and semiconducting SWNTs. In Chapter 3, we have explored graphite intercalated with $FeCl_3$.

It is worth pointing out that our approach can be employed to a large class of nanostructures, such as nanoribbons and bucky balls. The DFT calculations become routine for relevant systems. We plan to continue work with SWNTs of various diameters differing from what has been presented in this thesis. Examining geometry effects of electric bias and investigating band gap tunability on a wider range of SWNTs can substantiate our understanding of the electric bias influence on electronic structures. We will consider multiwall carbon nanotubes and also intercalating graphene with different atoms or molecules and investigate the effects of applying an electric bias. Functionalization of the graphene sheets is also of interest; adding more layers of graphene between intercalants may result in electric bias having a different effect on the electric properties of the compound. The availability of experimental collaboration will

be useful to test our predictions. Validating our computational results is not only practical but also necessary for investigating the structural and electronic characteristics in these systems.

REFERENCES

(*1*) K. S. Novoselov, A. K. Geim, S. V. Morozov, D. Jiang, Y. Zhang, S. V. Dubonos, I. V. Grigorieva, A. A. Firsov, *Science* **2004**, *306*, 666.

(*2*) K. S. Novoselov, A. K. Geim, S. V. Morozov, D. Jiang, M. I. Katsnelson, I. V. Grigorieva, S. V. Dubonos, A. A. Firsov, *Nature* **2005**, *438*, 197.

(*3*) Y. B. Zhang, Y. W. Tan, H. L. Stormer, P. Kim, *Nature* **2005**, *438*, 201.

(*4*) C. Berger, Z. M. Song, T. B. Li, X. B. Li, A. Y. Ogbazghi, R. Feng, Z. T. Dai, A. N. Marchenkov, E. H. Conrad, P. N. First, W. A. de Heer, *J. Phys. Chem. B* **2004**, *108*, 19912.

(*5*) S. Stankovich, D. A. Dikin, G. H. B. Dommett, K. M. Kohlhaas, E. J. Zimney, E. A. Stach, R. D. Piner, S. T. Nguyen, R. S. Ruoff, *Nature* **2006**, *442*, 282.

(*6*) A. Reina, X. T. Jia, J. Ho, D. Nezich, H. B. Son, V. Bulovic, M. S. Dresselhaus, J. Kong, *Nano Lett.* **2009**, *9*, 30.

(*7*) D. V. Kosynkin, A. L. Higginbotham, A. Sinitskii, J. R. Lomeda, A. Dimiev, B. K. Price, J. M. Tour, *Nature* **2009**, *458*, 872.

(*8*) D. Zhan, L. Sun, Z. H. Ni, L. Liu, X. F. Fan, Y. Wang, T. Yu, Y. M. Lam, W. Huang, Z. X. Shen, *Adv. Func. Mat.* **2010**, 20, 20

(*9*) C. T. White, J.W. Mintmire, *J. Phys. Chem. B.* **2005,** *109*, 52-65.

(*10*) R. Saito, G. Dresselhaus, M. S. Dresselhaus, *Phys. Prop. of Carbon Nanotubes* **1998,** 272.

(*11*) R. Saito, G. Fujita, G, Dresselhaus, M. S. Dresselhaus, *Appl. Phys. Lett.* **1992,** *60*, 2204-2206.

(*12*) M. S. Dresselhaus, G. Dresselhaus, R. Saito, *Phys. Rev. B.* **1992,** *45*, 6234-6242.

(*13*) X. Lu, Z. Chen, *Chem. Rev.* **2005,** 105, 10, 3643–3696.

(*14*) C. J. Cramer, *Essentials of Computaional Chemistry: Second Edition Theories and Models* **2004**, West Sussex: John Wiley & Sons, Ltd., 596.

(*15*) S. M. Bachrach, *Computational Organic Chemistry* **2007**, Hoboken: John Wiley &

Sons, Inc., 478.

(*16*) W. Kohn, A. D. Becke, R. G. Parr, *J. Phys. Chem.* **1996**, 100, 12974-12980.

(*17*) R. Parthasarathi, V. Subramanian, P. K. Chattaraj, Chem. Phys. Lett. **2003,** 382, 48.

(*18*) E. R. Davidson, B. E. Eichinger, B. H. Robinson, Opt. Mater. **2006**, 29, 360.

(*19*) C. Kim, B. Kim, Phys. Rev. B **2002**, 65, 165418.

(*20*) G. Zhou, W. H. Duan, B. L.Gu, Phys. Rev. Lett. **2001**, 87, 095504.

(*21*) B. Delley, J. Chem. Phys. **2000**, 113, 7756.

(*22*) DMol^3, Accelrys Software Inc., San Diego, CA, **2010**.

(*23*) C. He, P. Zhang, Y. F. Zhu, Q. Jiang, J. Phys. Chem. C **2008**, 112, 9045.

(*24*) Z. M. Ao, W. T. Zheng, Q. Jiang, Nanotechnology **2008**, 19, 275710.

(*25*) C. Liao, H. M. Chang, B. H. Yang, J. Appl. Phys. **2007**, 102, 084308.

(*26*) M. Meunier, N. Quirke, J. Chem. Phys. **2000**, 113,369.

(*27*) X. Wu, X. C. Zeng, Nano Res. **2008**, 1, 40.

(*28*) A. D. Becke, *J. Chem. Phys.* **1993**, 98, 5648.

(*29*) C. Lee, W. Yang, R. G. Parr, *Phys. Rev. B* **1988**, 37, 785.

(*30*) B. Delley, *J. Chem. Phys.* **1990,** 92, 508.

(*31*) B. Delley, *J. Chem. Phys.* **2000**, 113, 7756.

(*32*) X. Q. Wang, C. Z. Wang, B. L. Zhang, K. M. Ho, *Phys. Rev. Lett.* **1992**, 69, 69.

(*33*) X. Q. Wang, C. Z. Wang, K. M. Ho, *Phy. Rev. B.* **1995**, 51, 8656.

(*34*) M. S. Dresselhaus, G. Dresselhaus, *Adv. Phys.* **2002**, *51*, 1.

(*35*) T. E. Weller, M. Ellerby, S. S. Saxena, R. P. Smith, N. T. Skipper, *Nat. Phys.* **2005**, 1, 39.

(*36*) N. Emery, C. Herold, M. d'Astuto, V. Garcia, C. Bellin, J. F. Mareche, P. Lagrange, G. Loupias, *Phys. Rev. Lett.* **2005**, *95*, 087003.

(*37*) N. Jung, N. Kim, S. Jockusch, N. J. Turro, P. Kim, L. Brus, *Nano Lett.* **2009**, *9*, 4133.

(*38*) T. Abe, M. Inaba, Z. Ogumi, Y. Yokota, Y. Mizutani, *Phys. Rev. B* **2000**, *61*, 11344.

(*39*) W. Zhao, P. H. Tan, J. Liu, A. C. Ferrari, *J. Am. Chem. Soc.* **2011**, 133, 15, 5941–5946

(*40*) J. P. Perdew, K. Burke, Y. Wang, *Phys. Rev. B* **1996**, *54*, 16533.